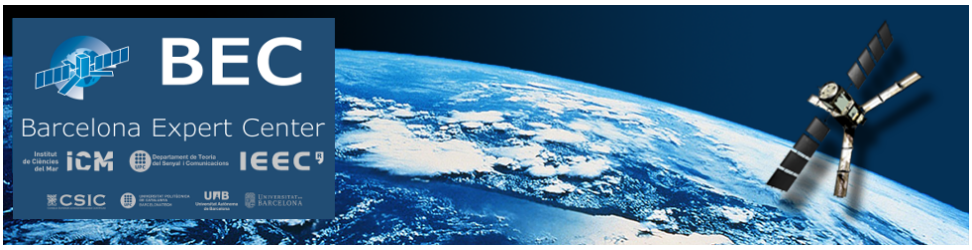

File: `BEC-SMOS-PD-SSSv2-v1.pdf` , version `1.0`

Title: Global SMOS-BEC SSS L3 and L4 Product v2 Description.

Authors: E. Olmedo, C. González-Haro, V. González-Gambau, J. Martínez, A. Turiel.

Contact: smos-bec@icm.csic.es

Date: 11/05/2020

GLOBAL SMOS-BEC SSS L3 AND L4 PRODUCT V2 DESCRIPTION

Abstract: This is the product specification document for the L3 and the L4 SMOS Sea Surface Salinity V2 produced and distributed by the BEC team through its data visualization and distribution service http://bec.icm.csic.es/bec-ftp-service/

Contents

1 INTRODUCTION

This is the product specification document for the L3 and the L4 global SMOS Sea Surface Salinity (SSS) V2 produced and distributed at BEC.

SMOS-BEC SSS products are generated following a debiased non-Bayesian approach presented in [Olmedo et al., 2017]. Version 2 of the global product includes the following improvements with respect to the previous version:

- New filtering criteria that is more geophysically consistent than the one applied to version 1 of the product (see section 2.1.6).
- Latitudinal bias correction following the approach presented in [Olmedo et al., 2019] (see section 2.2.2).
- New interpolation algorithms that aims to better preserve the salinity gradients, specially those close to the coast. Version 1 of the L3 global product was computed by using an objective analysis scheme with correlation radii of 175 km, 125 km and 75 km. Version 2 of the L3 product includes two different salinity fields: high resolution that consists of a binned salinity in a grid of $0.25^o \times 0.25^o$; and low resolution that applies a spatial smoothing windows of 50km to the previous salinity field (see section 2.2).
- An estimation of the salinity uncertainty (see section 2.1.7)
- A new scheme of L4 fusion that aims to better preserve salinity gradients close to the coast (see section 2.3).

2 SCIENCE ALGORITHM OVERVIEW

2.1 Level 2 Algorithms

We use the debiased non-Bayesian retrieval of SSS that was introduced in [Olmedo et al., 2017]. This approach aims to correct two known issues: the systematic biases caused by the presence of land masses and radio interference, and the data gaps due to the non-convergence of the retrieval algorithm.

2.1.1 Input data

The Brightness temperatures (TBs) obtained from SMOS MIRAS L1B TBs v620 provided by ESA are used as an input for the SMOS SSS retrieval. The L1B v620 product contains the Fourier coefficients of the measured brightness temperature. Starting from this product, using ESA's Earth Observation Customer Furnished Item (EOCFI) orbit propagation libraries [ESA, 2014] and following a similar procedure as the one used in the operational SMOS level 1 processor chain [Deimos, 2014], the measured TBs are obtained in the antenna reference frame (ARF). The unique difference from the standard processor is the number of points contained per snapshot (*i.e.* the resolution). The operational processor uses, at antenna level, a hexagonal grid of 128×128 points (*i.e.* $2^7 \times 2^7$). The projection of this antenna grid into the ground provides a resolution of about 15 km at bore-sight. This resolution is more than twice SMOS theoretical finer resolution [McMullan et al., 2008]. We have thus reduced the computational cost without actually losing information by using an antenna hexagonal grid of 64×64 ($2^6 \times 2^6$) points.

2.1.2 Forward Model

The forward model linking the modeled TB to SSS relies on the dielectric constant model proposed by Klein and Swift [Klein and Swift, 1977] which non-linearly depends on SSS and sea surface temperature (SST). Nevertheless, the measured TB not only contains information about brightness temperature of the flat sea, but also contributions due to other main sources: the roughness of the sea surface [Guimbard et al., 2012], the reflected emission of the atmosphere, the reflection on the sea surface of the galactic emission ([Tenerelli et al., 2008]) and the sun glitter [Reul et al., 2007]. Therefore, all these additional contributions to the TB term must be modeled at the bottom of the atmosphere (BOA) and then translated to the ARF prior to minimizing Eq. (1). Thus, the atmospheric attenuation effect over brightness temperature must be taken into account together with the direct emission of the atmosphere itself to estimate the modeled TB at the top of the atmosphere (TOA). Finally, to go from TOA to ARF, the ionosphere must be taken into account. The ionospheric effect translates into a rotation in the polarization components of TB. All these contributions are described in detail in Ocean SMOS Team (2016).

2.1.3 Non-Bayesian retrieval of SSS

We retrieve a single SSS value for each TB measurement, that is, along the same dwell line we have a value of SSS for each valid incidence angle, namely:

$$F^{j}_{non-Bayesian}(SSS) = \left[I^{meas}(\theta_j) - I(\theta_j, SSS, p_1, \ldots, p_{N_p})\right]^2, \quad (1)$$

where the super index j indicates one of the N_m available incidence angles. The term $I = (TB_v + TB_h)/2$, both for the forward modeled (section 2.1.2) and measured data, is the First Stokes parameter at BOA divided by 2; by summing up vertical (TB_v) and horizontal (TB_h) polarization we obtain a

term which is independent from Faraday rotation and simplifies its processing, although the retrieval could be done with each polarization independently. For the optimization, the other geophysical variables are given a fixed value, that of the geophysical priors p_k^0. We use as auxiliary data for setting the values of the priors the ones provided by the European Centre for Medium range Weather Forecast (ECMWF) ([Freitas, 2013] and [Sabater and De Rosnay, 2010]). For each Level 1B half-orbit an ECMWF auxiliary file (co-located in time and space with SMOS) is provided by ESA. We use the following fields for the retrieval: sea ice cover, sea surface temperature, rain rate, wave model 10 metre wind speed, 10 meters neutral equivalent wind (zonal and meridional components), significant height of wind waves, 2 meters air temperature, surface pressure, and vertically integrated total water vapour.

2.1.4 SSS systematic bias characterization: definition of a SMOS-based climatology

The characterization of the systematic bias (i.e. those that are not time dependent, but they depend on the acquisition conditions) is based on a classification of the non-Bayesian single-angle salinities retrievals. A first geophysical consistency filter on non-Bayesian salinities is applied: we discard any value out of the range $[0, 50]$. Then, the single-angle SSS values are grouped together according to their geolocation (latitude and longitude in a cylindrical grid of $0.25^o \times 0.25^o$, φ and λ), overpass direction (ascending or descending, denoted by a binary variable d), across-track distance to the center of swath (in 50-km bins, denoted by x) and incidence angle (in 5° bins, denoted by θ). For each given 5-tuple, $c = (\varphi, \lambda, d, x, \theta)$, we take all the retrievals $\{SSS(\varphi, \lambda, d, x, \theta)\}$ in the period we use (2011 to 2019) and construct the associated histograms (see Figure 1).

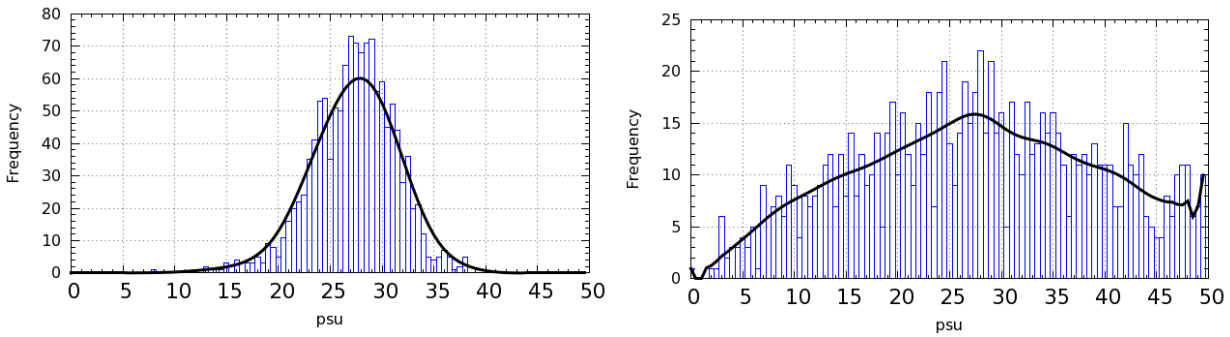

Figure 1: SMOS SSS histogram associated with $c = (20, -29, A, 225, 52)$ (left) and to $c = (31, 133, A, 275, 47)$ (right) (see the text for more details).

For every tuple, the corresponding SSS histogram is defined with bins of 0.5 psu. In order to improve the accuracy of the histogram and minimize the dependency on the histogram discretization, the mean of SSS inside each bin is considered as the representative value of SSS on that bin. The mode of the histograms are taken as a measure of the central reference value; the advantage of taking the mode, instead of other statistics, is that the mode is unaffected by the presence of outliers or by the skewness of the distribution.

The accuracy of the estimation of the mode of any histogram is relatively low, mainly because of the lack of sampling. To overcome this issue we have applied three times a weighted averaging window (with a size of seven points, including the central point, the three points to its left and the three points to its right) to each histogram to eliminate statistically non-significant fluctuations. As shown in Figure 1 (black line), this leads to a better determination of the location of the maximum probability (i.e., the mode). The resulting smoothed histogram is only used for estimating the mode; the rest of statistical parameters are computed from the original (not-smoothed) histogram. We

compute a SMOS-based climatological value for each given 5-tuple (denoted as $sss\_clim(\varphi, \lambda, d, x, \theta)$) by averaging all the retrieved single-angle SSSs in a range of $\pm\sigma$ around the estimated mode, where σ is the standard deviation of the single-angle SSSs for that 5-tuple.

Figure 2 shows two maps of the SMOS-based climatologies, corresponding to ascending overpasses, $x = 0$ km, $\theta = 5°$ (top) and $\theta = 35°$ (bottom). Significant differences are found for different θ values (that is, depending on the relative position of the pixel in the ARF).

2.1.5 Spatial bias correction

The single-angle SSS retrievals are corrected with their corresponding SMOS-based climatological value (sss_{clim}), thus creating a set of so-called SMOS-based anomalies (sss_{an}):

$$sss_{an}(\varphi, \lambda, d, x, \theta) = SSS(\varphi, \lambda, d, x, \theta) - sss_{clim}(\varphi, \lambda, d, x, \theta). \quad (2)$$

In order to obtain the value of SSS, a time-independent reference SSS value must be added to the sss_{an}. We use here the annual SSS climatology provided by the World Ocean Atlas 2013 (WOA2013) at $0.25^o \times 0.25^o$ (average decadal product, which is accessible at [National Oceanographic Data Center, 2013] [Zweng et al., 2013]).

2.1.6 SSS filtering criteria for non-Bayesian approach

We apply the following filtering criteria to discard poor quality values. For a given 5-tuple, $c = (\varphi, \lambda, d, x, \theta)$, a SMOS-climatological value is discarded and hence all related single-angle SSS retrievals, when the associated histogram suffers from one or more of the following conditions:

- It has less than 100 measurements;
- Its standard deviation is greater than 10 psu;
- The absolute value of its normalized skewness is greater than 1;
- Its kurtosis is lower than 2

As an example, see the two histograms displayed in Figure 1. The one in the left is accepted, as none of the conditions above is verified (it has 581 measurements, a standard deviation of 2.31, skewness equal to 0.97 and kurtosis equal to 3.74). The one in the right has 369 measurements, a standard deviation 5.82 and a 0.19 skewness, which are right, but its kurtosis (1.79) is too low and, therefore, it is discarded.

For the salinity retrievals that belong to a valid histogram, two additional filtering criteria are applied:

- The salinity retrieval is discarded when the corresponding SMOS-based anomaly is greater than

$$\sqrt{\sigma_c^2 + 25\sigma_{sss}^2(\varphi, \lambda)} \quad (3)$$

  with σ_c the standard deviation of the distribution associated to c and σ_{sss}^2 geophysical variability of the salinity at (φ, λ).

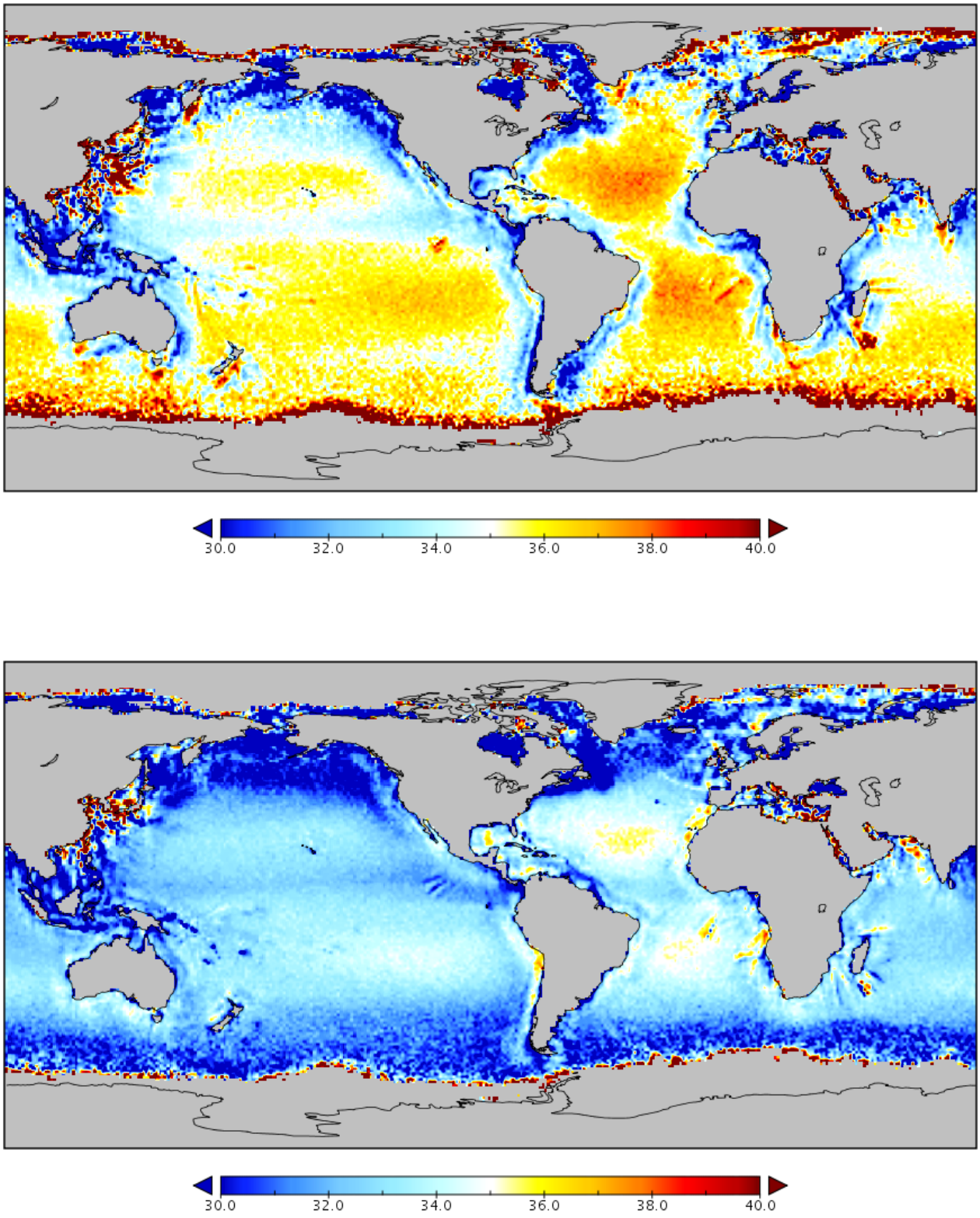

Figure 2: SMOS-based climatology for ascending overpasses and $x = 0$ km and $\theta = 5°$ (top) and $x = 0$ km and $\theta = 35°$ (bottom).

- For those salinity values that are valid after the previous filtering criteria, we temporally and spatially collocate the retrievals (by mixing different acquisition conditions) in 9-day maps at $0.25^o \times 0.25^o$. We consider as valid salinity measurements only those satisfying:

$$|s_0^{t,s} - \bar{s}^{t,s}| < \sigma^{t,s}, \tag{4}$$

with $\bar{s}^{t,s}$ the mean of all the temporal and spatial collocated $s_0^{t,s}$ retrievals and $\sigma^{t,s}$ the standard deviation of $s_0^{t,s}$.

2.1.7 Estimation of the Sea Surface Salinity uncertainty

The estimated sea surface salinity error is computed using with the next expression:

$$\epsilon = \frac{1}{2}\frac{(\sigma_H + \sigma_V)}{TB'} \tag{5}$$

where the σ_H and σ_V are the radiometric sensitivities for H and V polarized TB, respectively, and TB' is the derivative of the modelled TB First Stokes with respect to the salinity.

2.2 L3 Algorithm

We temporally and spatially collocate the retrievals corrected by algorithms shown in section 2.1.5 and filtered with the criteria described in section 2.1.6 by mixing different acquisition conditions in 9-day maps at $0.25^o \times 0.25^o$. Two different salinity fields are provided:

- High resolution salinity: binned salinity field corresponding to the average of the salinity values retrieved during the 9-day period of the map at the corresponding cell of $0.25^o \times 0.25^o$.
- Low resolution salinity: smoothed salinity field corresponding to a gaussian filter of 50km of the binned salinity value.

2.2.1 Temporal bias mitigation

We apply a temporal bias correction that is based on imposing that the SMOS-based anomaly L3 maps (generated for a given time period T) have zero mean over the global ocean. From the physical point of view, this correction (i.e., requiring the cancellation of the spatial average of the SSS anomaly on a given region) is equivalent to assume that the amount of salt at surface layer does not change with time in the global ocean.

Then, the global L3 SSS map is corrected by subtracting the mean of the SMOS-based anomalies on the global ocean, in the following way.

$$SSS^T_{corr.an}(\varphi, \lambda) = SSS^T_{an}(\varphi, \lambda) - M^T \tag{6}$$

where M^T is the average anomaly on the global ocean for the period T, namely:

$$M^T = \frac{\Sigma_{\text{valid}\varphi,\lambda} SST^T_{an}(\varphi, \lambda)}{N^T} \tag{7}$$

with N^T the number of grid points with valid φ, λ during T.

2.2.2 Latitudinal and seasonal bias mitigation

Afer the temporal correction, the L3 maps are still affected by a latitudinal and seasonal contamination [Martín-Neira et al., 2016]. We apply the following latitudinal and seasonal bias correction:

- We compute a monthly SMOS climatology from the L3 9-day maps, $\bar{s}_0$.
- We subtract the montly WOA climatology, $\Delta\bar{s}_0 = \bar{s}_0 - s^{WOA}$.
- We fit $\Delta\bar{s}_0$ by a parabolic function of the latitude. $\Delta\bar{s}_0 \approx \bar{a}_{m,\varphi}\varphi^2 + \bar{b}_{m,\varphi}\varphi + \bar{c}_{m,\varphi}$
- In order to compute the final 9-day SMOS SSS map, $\bar{a}_{m,\varphi}$, $\bar{b}_{m,\varphi}$ and $\bar{c}_{m,\varphi}$ are daily interpolated to the central epoch of the 9-day SMOS SSS map. We denotate the SMOS SSS maps after applying the latitudinal and seasonal bias correction as s.

2.2.3 Spatial residual bias mitigation

After applying all the previously described corrections, we make a last check. By definition (see section 2.1.5) the average of the retrieved salinity for the full period (2011-2019) should be equal to the multiyear reference used in the generation of the salinity, i.e. WOA2013 at each geographical location. We found significant differences between both averages, that may be due to an inaccurate SMOS-based climatology. This may happen when the SMOS-based histograms are far from Gaussian and then differences between the mode (used here as central estimator of the histogram) and the mean of all salinity retrievals after applying the filtering criteria are significant. In order to mitigate this, we remove the map corresponding to the difference between the mean average of all the SMOS SSS in the 2011-2019 period and WOA13 (see Figure 3).

2.3 L4 Algorithm

Singularity analysis based fusion ([Umbert et al., 2014] and [Olmedo et al., 2016]) can be used not only to improve the signal level, but also to increase the spatial and temporal resolution of fused maps, provided that the template (OSTIA SST for us) has a better spatial and temporal resolutions than the L3 SSS maps. Assuming that both variables have the same singularity exponents ([Turiel et al., 2005] and [Turiel et al., 2008]), we impose the following local relationship:

$$SSS = a \times SST + b \tag{8}$$

where a and b are expected to have small gradients. The parameters a and b are computed by using a local weighting average (see [Umbert et al., 2014] and [Olmedo et al., 2016] for more details). Taking advantage of the fact that a and b do not have sharp variations over large regions, the evaluation of a and b is performed as the linear regression coefficients using as local averaging:

$$< f >_x = \frac{1}{\sum_{x' \neq x} \frac{1}{|x'-x|^4}} \sum_{x' \neq x} \frac{f(x')}{|x'-x|^4}. \tag{9}$$

We use the same weighted average as in [Olmedo et al., 2016], that is the inverse of th 4-th power of the distance to the central point. In order to better describe the small scale features, we modify the last formulation as follows:

$$< f >_x = \frac{1}{\sum_{0<|x'-x|<2.5^o} \frac{1}{|x'-x|^4}} \sum_{0<|x'-x|<2.5^o} \frac{f(x')}{|x'-x|^4} \tag{10}$$

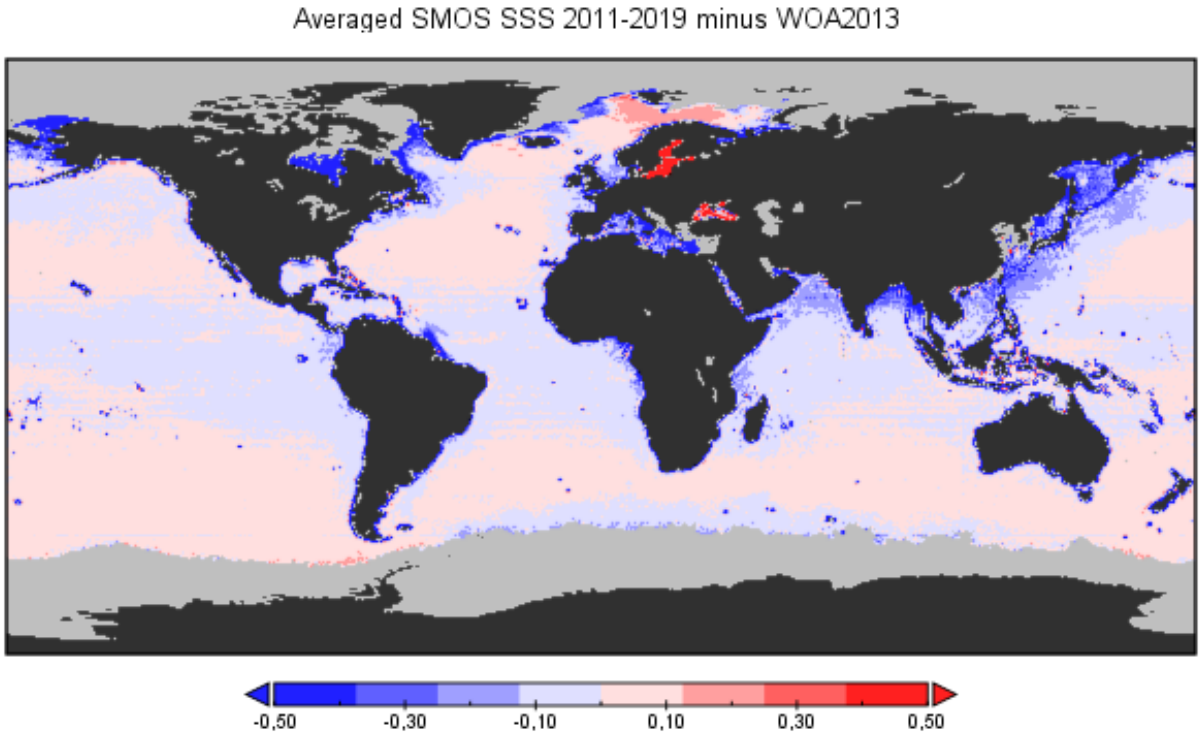

Figure 3: Difference between the 2011-2019 average of SMOS BEC SSS maps after applying corrections described in sections 2.1.5, 2.2.1 and 2.2.2 and WOA2013 SSS.

We use OSTIA SST daily maps at $0.05^o \times 0.05^o$ (see [Donlon et al., 2012]) as a template to increase the spatial and temporal resolution of the L3 SMOS SSS maps. As a result, the SMOS L4 SSS product has a daily temporal resolution and it is provided in a spatial grid of $0.05^o \times 0.05^o$. Hereafter we refer to this product as SMOSBECL4.

3 GLOBAL SSS PRODUCTS

The L3 product contains the high resolution (corresponding to the binned salinity value) and low resolution (correspondig to the smoothed salinity value) SSS in the corresponding 9-day period at each $0.25^o \times 0.25^o$ cell, and it is daily generated. This product also contains an estimation of the sea surface salinity uncertainty.

The L4 product is provided in a grid of $0.05^o \times 0.05^o$ in and with daily temporal resolution.

3.1 File naming convention

The resulting Level 3 and Level 4 products are distributed in netCDF format and the name of each file follows the layout:

```
BEC_SSS___SMOS__GLO_LL__X_YYYYMMDDTHHMMSS_GGGGU_TT_DDD_vVVV.nc
```

where each field of the filename is as follows:

- BEC: indicates the institution (Barcelona Expert Centre, BEC),
- SSS: stands for Sea Surface Salintiy
- SMOS: stands for Soil Moisture and Ocean Salinity,
- GLO: indicates the region, Global,
- LL: indicates the level (L3, L4),
- X: indicates the half-orbit type,
  - A: ascending,
  - D: descending,
  - B: both,
- YYYYMMDDTHHMMSS: central date of the file,
- GGGGU: indicates the spatial resolution of the grid and the unit,
  - 0.25d: LAT/LON regular grid of 1/4 degree.
- TT: indicates the temporal coverage of the data,
  - 9d: 9 days,
- DDD: delay processing mode: NRT for Near Real Time and REP for reprocessed.
- vVVV: version number

3.2 Data Definition

3.2.1 L3 product

The structure of the netCDF files with its dimensions, variables and global attributes is detailed here:

```
 dimensions:
     lat = 720 ;
     lon = 1400 ;
     time = UNLIMITED ; // (1 currently)
variables:
     float time(time) ;
        time:standard_name = "time" ;
        time:long_name = "Time" ;
        time:units = "seconds since 1970-1-1 00:00:00" ;
        time:time = "T" ;
        time:calendar = "gregorian" ;
     float lat(lat) ;
        lat:standard_name = "latitude" ;
        lat:long_name = "Latitude" ;
        lat:units = "degrees_north" ;
        lon:axis = "Y" ;
     float lon(lon) ;
```

```
        lon:standard_name = "longitude" ;
        lon:units = "degrees_east" ;
        lon:long_name = "longitude" ;
        lon:axis = "X" ;
    int crs ;
        crs:longitude_of_prime_meridian = 0.f ;
        crs:semi_major_axis = 6378137.f ;
        crs:inverse_flattening = 298.2572f ;
        crs:proj4tex= "+proj=latlong +ellps=WGS84" ;
        crs:grid_mapping_name = "latitude_longitude" ;
        crs:datum = "WGS84" ;
    float uncertainty_sss(time, lat, lon) ;
        uncertainty_sss:units = "1" ;
        uncertainty_sss:standard_name = "uncertainty_sea_surface_salinity" ;
        uncertainty_sss:long_name = "Sea Surface Salinity Uncertainty" ;
        uncertainty_sss:description = "Practical Sea Surface Salinity [psu]" ;
        uncertainty_sss:grid_mapping = "crs" ;
        uncertainty_sss:valid_min = 0.f ;
        uncertainty_sss:valid_max = 50.f ;
        uncertainty_sss:missing_value = -999.f ;
        uncertainty_sss:_FillValue = -999.f ;
    float lr_sss(time, lat, lon) ;
        lr_sss:standard_name = "low_resolution_sea_surface_salinity" ;
        lr_sss:long_name = "Low Resolution Sea Surface Salinity" ;
        lr_sss:units = "1" ;
        lr_sss:description = "Smoothed Sea Surface Salinity in Practical Salinity Units
[psu]" ;
        lr_sss:missing_value = -999.f ;
        lr_sss:_FillValue = -999.f ;
        lr_sss:grid_mapping = crs ;
        lr_sss:valid_min = 0.f ;
        lr_sss:valid_max = 50.f ;
    float hr_sss(time, lat, lon) ;
        hr_sss:standard_name = "high_resolution_sea_surface_salinity" ;
        hr_sss:long_name = "High Resolution Sea Surface Salinity" ;
        hr_sss:units = "1" ;
        hr_sss:description = "Binned Sea Surface Salinity in Practical Salinity Units
[psu]" ;
        hr_sss:missing_value = -999.f ;
        hr_sss:_FillValue = -999.f ;
        hr_sss:grid_mapping = crs ;
        hr_sss:valid_min = 0.f ;
        hr_sss:valid_max = 50.f ;
global attributes:
        :Conventions = "CF-1.6" ;
        :date_created = "2019-12-15 09:30:48 GMT" ;
        :geospatial_lon_resolution = 0.25f ;
        :geospatial_lat_resolution = 0.25f ;
        :geospatial_lon_units = "degrees_east" ;
```

:geospatial_lat_units = "degrees_north" ;
:geospatial_lon_min = -180.f ;
:geospatial_lon_max = 180.f ;
:geospatial_lat_min = -90.f ;
:geospatial_lat_max = 90.f ;
:time_coverage_start = "2011-12-18T0:00:00" ;
:time_coverage_end = "2011-12-26T23:59:59" ;
:institution = "Barcelona Expert Center (BEC), ICM-CSIC, Barcelona, Spain" ;
:title = "SMOS BEC global SSS product v2" ;
:copyright = "BEC research products are freely distributed. If this data is used for publication, the following ackowlegment should be included: These data were produced by the Barcelona Expert Centre (http://bec.icm.csic.es/). The Barcelona Expert Center is a joint initiative of the Spanish Research Council (CSIC) and Technical (University of Catalonia (UPC), mainly founded by the Spanish National Program on Space." ;
:references = "SSS have been retrieved following the algorithm described in Olmedo, E. et al., De-biased non-Bayesian Retrieval: a novel approach to SMOS Sea Surface Salinity, Remote Sensing of Environment 193 (2017) 103â126 and Olmedo, E. et al.,CHARACTERIZATION AND CORRECTION OF THE LATITUDINAL AND SEASONAL BIAS IN BEC SMOS SEA SURFACE SALINITY MAPS, 2019, Proceedings of IGARSS 2019 (Paper number WE4.R12.4). Specific publication describing the entire methodology and the performance of the product has been submitted in Earth System Science Data journal, Olmedo, E. et al., Nine years of SMOS Sea Surface Salinity global maps at the Barcelona Expert Center" ;
:project = "This product has been developed as part of the Copernicus Marine Environment Monitoring Service (CMEMS) Land-Marine Boundary Development and Analysis (Lambda) project." ;
:funding = "The development was also supported by the Ministry of Economy and Competitiviness, Spain, through the National R+D Plan under L-Band Project ESP2017-89463-C3-1- and previous grants and by the European Space Agency by means of the contract CCI+ Salinity." ;
:product_version = "2.0" ;
:url = "http://bec.icm.csic.es" ;
:creator_mail = "smos-bec@icm.csic.es" ;
:sensor = "SMOS/MIRAS" ;
:platform = "PROTEUS" ;
:license = "This product is distributed under Creative Commons Attribution license (CC BY 4.0).You are free to share and adapt this product under the following terms:You must give appropriate credit (see copyright), provide a link to the license, and indicate if changes were made. You may do so in any reasonable manner, but not in any way that suggests the licensor endorses you or your use." ;
:license_url = "https://creativecommons.org/licenses/by/4.0/" ;
:comment = "These data were produced at BEC as part of the Lambda project. Please, send your feedback to olmedo@icm.csic.es" ;

3.2.2 L4 product

The structure of the netCDF files with its dimensions, variables and global attributes is detailed here:

dimensions:
lat = 3600 ;

```
     lon = 7200 ;
     time = UNLIMITED ; // (1 currently)
variables:
     float time(time) ;
        time:standard_name = "time" ;
        time:long_name = "Time" ;
        time:units = "seconds since 1970-1-1 00:00:00" ;
        time:time = "T" ;
        time:calendar = "gregorian" ;
     float lat(lat) ;
        lat:standard_name = "latitude" ;
        lat:long_name = "Latitude" ;
        lat:units = "degrees_north" ;
        lon:axis = "Y" ;
     float lon(lon) ;
        lon:standard_name = "longitude" ;
        lon:units = "degrees_east" ;
        lon:long_name = "longitude" ;
        lon:axis = "X" ;
     float sss(time, lat, lon) ;
        sss:units = "1" ;
        sss:standard_name = "sea_surface_salinity" ;
        sss:long_name = "Level 4 Sea Surface Salinity" ;
        sss:description = "Level 4 Sea Surface Salinity in Practical Salinity Units [psu]"
;
        sss:missing_value = -999.f ;
        sss:_FillValue = -999.f ;
global attributes:
        :title = "Global SMOS Level 4 Sea Surface Salinity file" ;
        :institution = "Barcelona Expert Center (BEC), ICM-CSIC, Barcelona, Spain" ;
        :references = "SSS have been retrieved following the algorithm described in Olmedo,
E. et al., De-biased non-Bayesian Retrieval:  a novel approach to SMOS Sea Surface Salinity,
Remote Sensing of Environment 193 (2017) 103â126, Olmedo, E. et al.,CHARACTERIZATION AND
CORRECTION OF THE LATITUDINAL AND SEASONAL BIAS IN BEC SMOS SEA SURFACE SALINITY MAPS,
2019, Proceedings of IGARSS 2019 (Paper number WE4.R12.4).  The multifractal fusion method
is described in Olmedo, E. et al., Improving time and space resolution of SMOS salinitymaps
using multifractal fusion, Remote Sensing of Environment 180 (2016) 246â263.  Specific
publication describing the entire methodology and the performance of the product has been
submitted in Earth System Science Data journal, Olmedo, E. et al., Nine years of SMOS
Sea Surface Salinity global maps at the Barcelona Expert Center" ;
        :copyright = "BEC research products are freely distributed.  If this data is
used for publication, the following ackowlegment should be included:  These data were
produced by the Barcelona Expert Centre (http://bec.icm.csic.es/).  The Barcelona Expert
Center is a joint initiative of the Spanish Research Council (CSIC) and Technical (University
of Catalonia (UPC), mainly founded by the Spanish National Program on Space." ;
        :Conventions = "CF-1.4" ;
        :date_created = "2020-02-06 04:12:18 GMT" ;
        :geospatial_lon_resolution = 0.05f ;
        :geospatial_lat_resolution = 0.05f ;
```

```
        :geospatial_lon_min = -180.f ;
        :geospatial_lon_max = 180.f ;
        :geospatial_lat_min = -90.f ;
        :geospatial_lat_max = 90.f ;
        :description = "BEC L4 product resulting from singularity analysis BEC binned
L3 product and sea surface temperature (SST) provided daily by Operational Sea Surface
Temperature and Sea Ice Analysis (OSTIA) system.  Visit http://ghrsst-pp.metoffice.com/pages/l
for additional information about OSTIA system" ;
        :time_coverage_start = "2011-04-01T0:00:00" ;
        :time_coverage_end = "2011-04-01T23:59:59" ;
        :project = "This product has been developed as part of the Copernicus Marine
Environment Monitoring Service (CMEMS) Land-Marine Boundary Development and Analysis (Lambda)
project." ;
        :funding = "The development was also supported by the Ministry of Economy and
Competitiviness, Spain, through the National R+D Plan under L-Band Project ESP2017-89463-C3-1-
and previous grants and by the European Space Agency by means of the contract CCI+ Salinity."
;
        :product_version = "2.0" ;
        :url = "http://bec.icm.csic.es" ;
        :creator_mail = "smos-bec@icm.csic.es" ;
        :sensor = "SMOS/MIRAS" ;
        :platform = "PROTEUS" ;
        :license = "This product is distributed under Creative Commons Attribution license
(CC BY 4.0).You are free to share and adapt this product under the following terms:You
must give appropriate credit (see copyright), provide a link to the license, and indicate
if changes were made.  You may do so in any easonable manner, but not in any way that
suggests the licensor endorses you or your use." ;
        :license_url = "https://creativecommons.org/licenses/by/4.0/" ;
        :comment = "These data were produced at BEC as part of the Lambda project.  Please,
send your feedback to olmedo@icm.csic.es" ;
```

3.3 Data Access

The Global SMOS SSS v2.0 produced at BEC is freely available through a SFTP server. If your browser is SFTP compatible you can browse directly from sftp://becftp.icm.csic.es:27500 address. The data can be download after completing registration in our BEC ftp service (http://bec.icm.csic.es/bec-ftp-service-registration/). For more information about the BEC ftp service, please visit http://bec.icm.csic.es/bec-ftp-service/. For any further assistance, contact to smos-bec@icm.csic.es.

The following diagram tree shows the complete path to the Global SMOS SSS v2.0 repository.

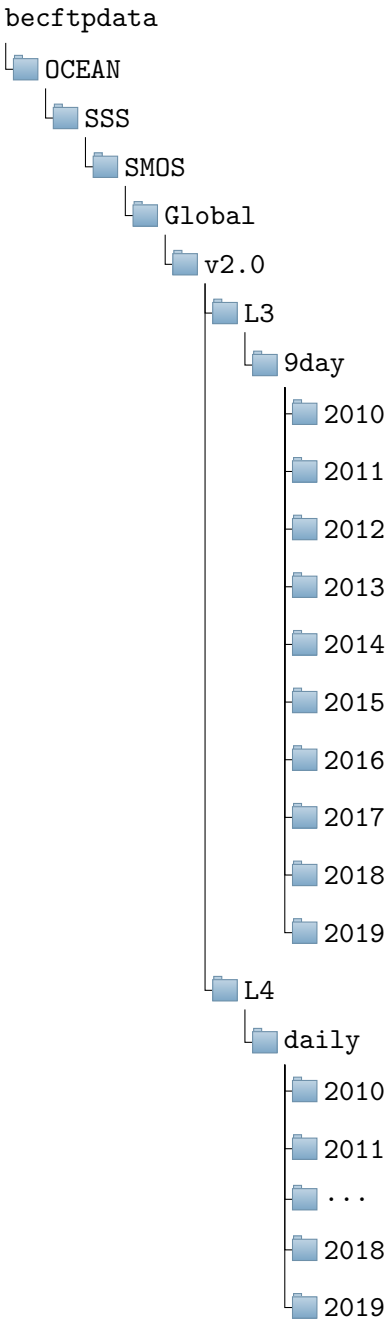
becftpdata
OCEAN
SSS
SMOS
Global
v2.0
L3
9day
2010
2011
2012
2013
2014
2015
2016
2017
2018
2019
L4
daily
2010
2011
...
2018
2019

A QUALITY ASSESSMENT

The aim of this section is to report the performance of the SMOS BEC SSS global products v2 (L3 and L4). For this, we compute the differences between the SMOS BEC SSS products and the Argo data. We also include the SMOS BEC global product v1 to compare its performance with the one of the new product. Table 1 summarizes the products that are assessed in this section. Notice that while the available time period for the SMOS BEC v2 is 2011-2019, the SMOS BEC v1 is only available for the period 2011-2016.

Name	**Description**	**Frequency**	**Average Period**	**Grid**	**Orbit**
L3v1	L3 Global product v1	daily	9 days	$0.25^o \times 0.25^o$	both
HR	L3 v2: high resolution	daily	9 days	$0.25^o \times 0.25^o$	both
LR	L3 v2: low resolution	daily	9 days	$0.25^o \times 0.25^o$	both
L4v1	L4 Global product v1	daily	daily	$0.05^o \times 0.05^o$	both
L4	L4 Global product v2	daily	daily	$0.05^o \times 0.05^o$	both

Table 1: Ocean products used in this report.

Name	Description	Latitude	Longitude
SEP	Region in the South Eastern Pacific	30^oS - 0^oN	150^oW - 120^oW
EQU	Equatorial oceans	10^oS - 10^oN	All
TRO	Tropics	30^oS - 30^oN	All
GLO	Tropics and mid-latitudes	60^oS - 60^oN	All
NAT	Region in the North Atlantic	30^oN - 50^oN	50^oW -0^oW
EAT	Region in the Equatorial Atlantic	0^oN - 20^oN	70^oW - 40^oW
EPA	Region in the Equatorial Pacific	10^oS - 10^oN	180^oW - 80^oW
NPA	Region in the North Pacific	30^oN - 50^oN	180^oW - 120^oW
SAT	Region in the South Atlantic	40^oS - 0^oN	30^oW - 0^oW
IND	Region in the Indian Ocean	30^oS - 0^oN	60^oE - 120^oE

Table 2: Zones under study

A.1 Argo

The SMOS-BEC products are compared in this section with in situ data. The statistical comparison is carried out with close-to-surface values acquired by Argo floats (Argo float data and metadata from Global Data Assembly Centre (Argo GDAC). SEANOE. http://doi.org/10.17882/42182).

In particular, we consider the uppermost Argo salinity value to compare with SMOS. Only profiles with valid values between 10m and 5m depth are considered. The differences between satellite and Argo salinity are estimated in the regions defined in table 2.

Table 3 presents the statistics of the differences SMOS minus Argo salinity for the SMOS products described in Table 1 and the ocean regions GLO and TRO (as defined in table 2). The statistics are provided in a yearly basis. In terms of mean differences with respect to Argo, the new L3 product (HR and LR) provides very similar performance as the L3 v1 in GLO and slightly better in TRO. The SMOS BEC SSS product provides an average of the mean difference with respect to Argo bellow 0.02 and 006 PSU, in GLO and in TRO regions, respectively. Regarding the standard deviations of the differences with respect to Argo salinity, among the three salinity fields of the product v2, HR is the one with the largest standard deviation and L4 the one with the lowest standard deviation. This is something expected: HR is computed by a simple averaging; LR is the HR with a smoothing windows of 50km, so a reduction in the noise of the product is expected; and the techniques of fusion that are applied to the L4 also allow reducing the white noise of the salinity maps. In comparison with the previous product, the new version SMOS BEC v2 presents slightly higher standard deviation. This is also something expected. The new SMOS BEC product includes a new filtering criteria that is more permissive than the one used in the generation of v1. Moreover, the objective analysis scheme used in the generation of SMOS BEC product v1 produced also an over smoothing.

The benefits of using the new filtering criteria and the new interpolation schemes are observed in those regions with a larger salinity dynamics as the Equatorial Pacific, Equatorial Atlantic and Indian Ocean. In Figures 4, 5, 6, 7, 8 and 9, the regional statistics with respect to to Argo are provided for the period 2011-2016 (respectively).

Figure 10 shows the temporal evolution of the mean differences between every SMOS BEC product and Argo salinity in latitudinal bands of 0.25^o. The latitudinal and seasonal bias that affected to the SMOS BEC product v1 is partially mitigated in SMOS BEC product v2.

		SMOS - ARGO in GLO			**SMOS - ARGO in TRO**		
Year	Product	<Mean>	<STD>	<RMS>	<Mean>	<STD>	<RMS>
2011	L3v1	0.02	0.24	0.24	0.05	0.23	0.24
	HR	-0.02	0.34	0.34	-0.03	0.31	0.31
	LR	-0.02	0.27	0.27	-0.03	0.25	0.25
	L4v1	-0.00	0.20	0.20	0.03	0.22	0.22
	L4	-0.02	0.22	0.22	-0.04	0.21	0.21
2012	L3v1	0.02	0.24	0.24	0.05	0.23	0.24
	HR	-0.02	0.34	0.34	-0.04	0.31	0.31
	LR	-0.02	0.27	0.27	-0.04	0.25	0.26
	L4v1	-0.00	0.19	0.19	0.03	0.22	0.22
	L4	-0.02	0.22	0.23	-0.05	0.21	0.22
2013	L3v1	0.02	0.24	0.24	0.05	0.24	0.25
	HR	-0.03	0.34	0.34	-0.03	0.33	0.33
	LR	-0.02	0.27	0.27	-0.03	0.27	0.27
	L4v1	-0.01	0.19	0.19	0.02	0.22	0.22
	L4	-0.03	0.23	0.23	-0.04	0.22	0.23
2014	L3v1	0.03	0.25	0.25	0.07	0.25	0.26
	HR	-0.01	0.34	0.34	-0.02	0.32	0.32
	LR	-0.01	0.27	0.27	-0.02	0.27	0.27
	L4v1	0.00	0.21	0.21	0.04	0.24	0.24
	L4	-0.02	0.23	0.23	-0.03	0.23	0.23
2015	L3v1	0.03	0.25	0.25	0.09	0.26	0.27
	HR	-0.00	0.34	0.34	0.00	0.32	0.33
	LR	-0.00	0.28	0.28	0.00	0.27	0.27
	L4v1	0.00	0.22	0.22	0.05	0.24	0.25
	L4	-0.01	0.23	0.23	-0.01	0.23	0.23
2016	L3v1	0.02	0.27	0.27	0.08	0.27	0.29
	HR	-0.01	0.34	0.34	0.01	0.32	0.33
	LR	-0.01	0.28	0.28	0.01	0.27	0.28
	L4v1	-0.01	0.23	0.23	0.05	0.26	0.26
	L4	-0.02	0.24	0.24	0.00	0.24	0.24
2017	HR	0.00	0.28	0.28	0.03	0.27	0.27
	LR	-0.00	0.24	0.24	0.03	0.24	0.24
	L4	-0.00	0.22	0.22	0.02	0.22	0.22
2018	HR	0.01	0.27	0.27	0.04	0.26	0.26
	LR	0.01	0.24	0.24	0.04	0.23	0.23
	L4	0.01	0.21	0.21	0.03	0.21	0.21
2019	HR	0.02	0.27	0.27	0.06	0.25	0.26
	LR	0.02	0.24	0.24	0.06	0.23	0.23
	L4	0.02	0.21	0.21	0.05	0.21	0.21

Table 3: Statistics of the comparison with Argo

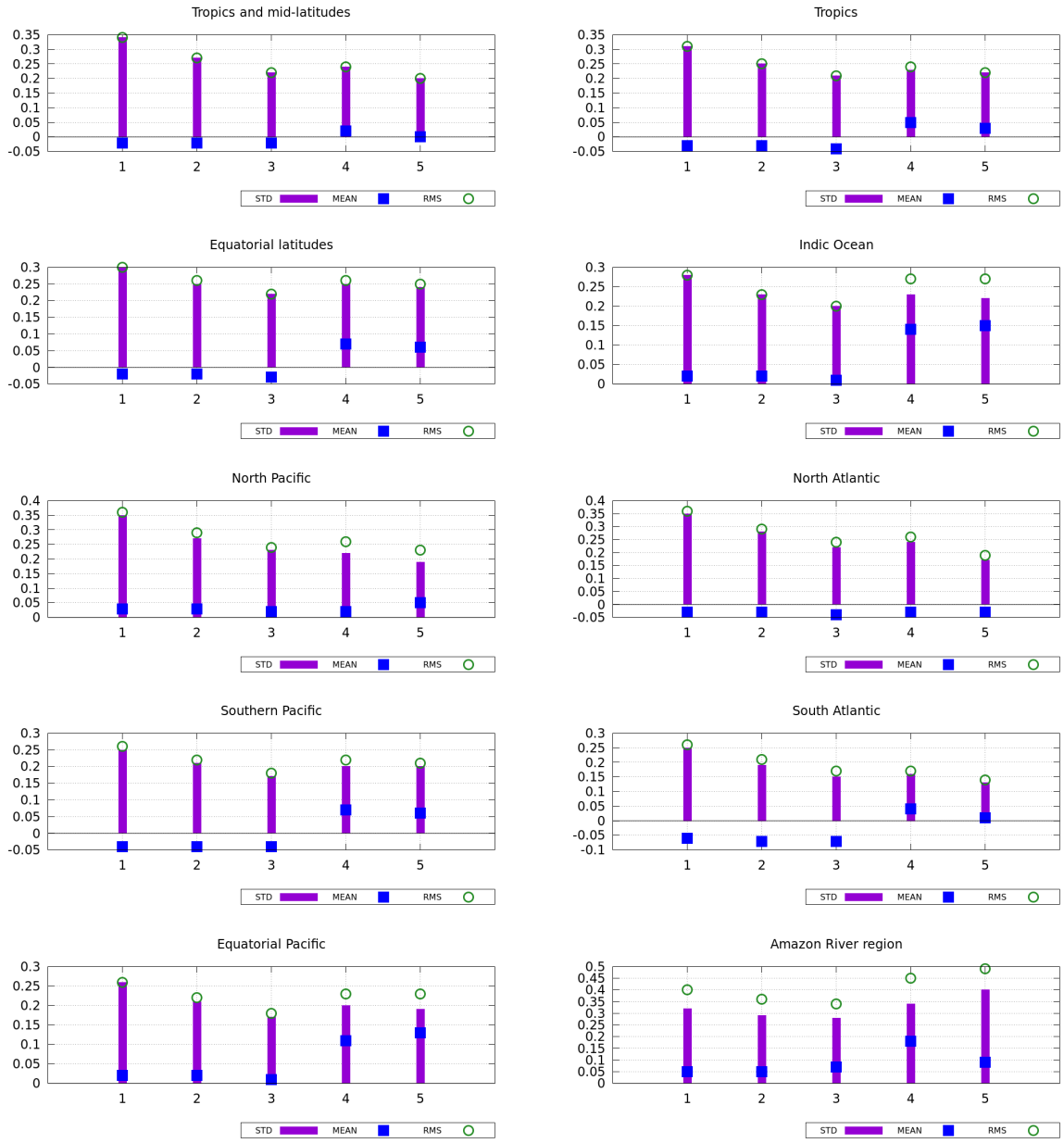

Figure 4: Regional statistics of differences of the different SMOS BEC SSS with respect to Argo salinity for the year 2011. Index 1 corresponds to the statistics of HR; 2 corresponds to LR; 3 to L4; 4 to L3V1; and 5 to L4V1.

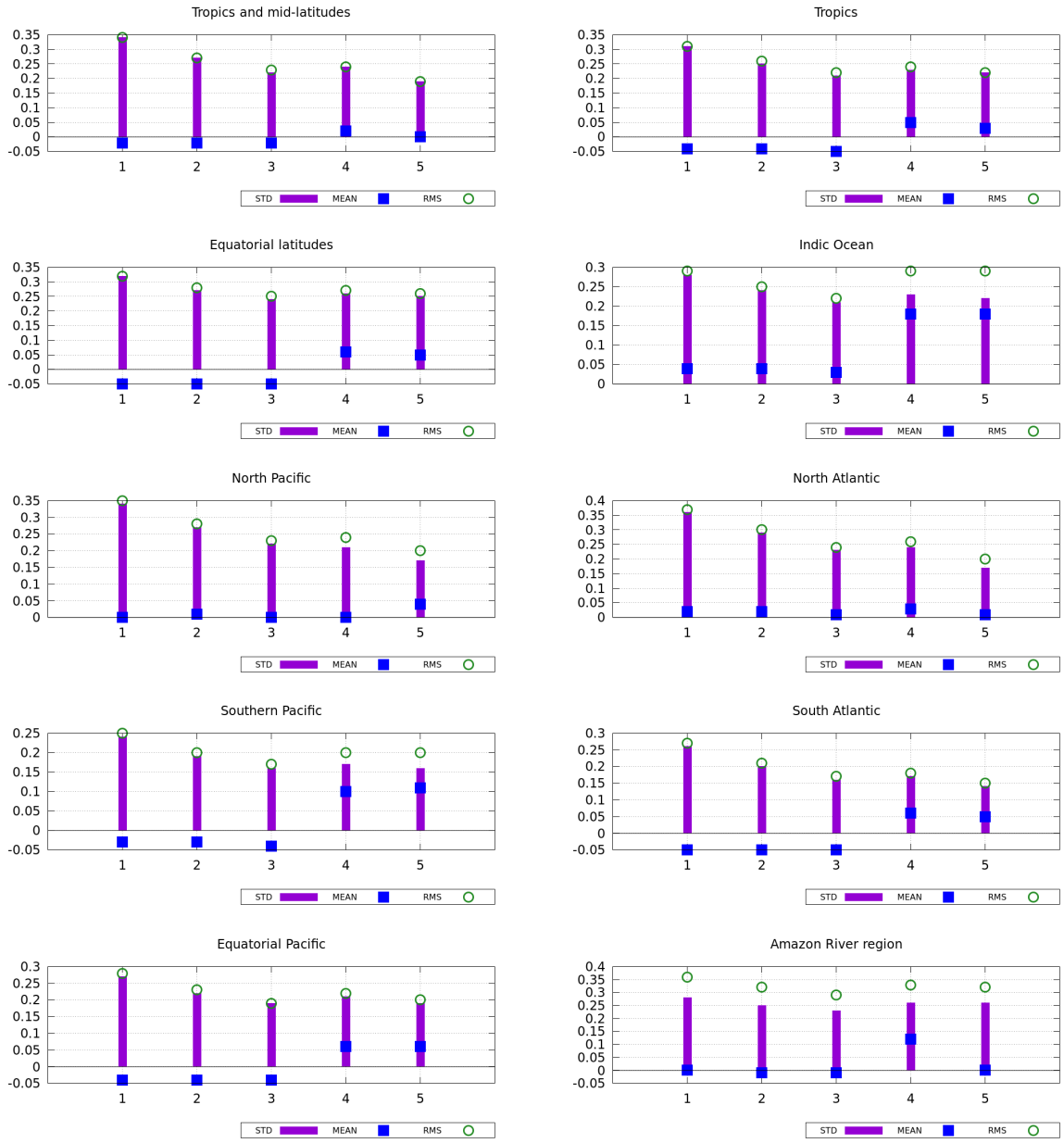

Figure 5: Regional statistics of differences of the different SMOS BEC SSS with respect to Argo salinity for the year 2012. Index 1 corresponds to the statistics of HR; 2 corresponds to LR; 3 to L4; 4 to L3V1; and 5 to L4V1.

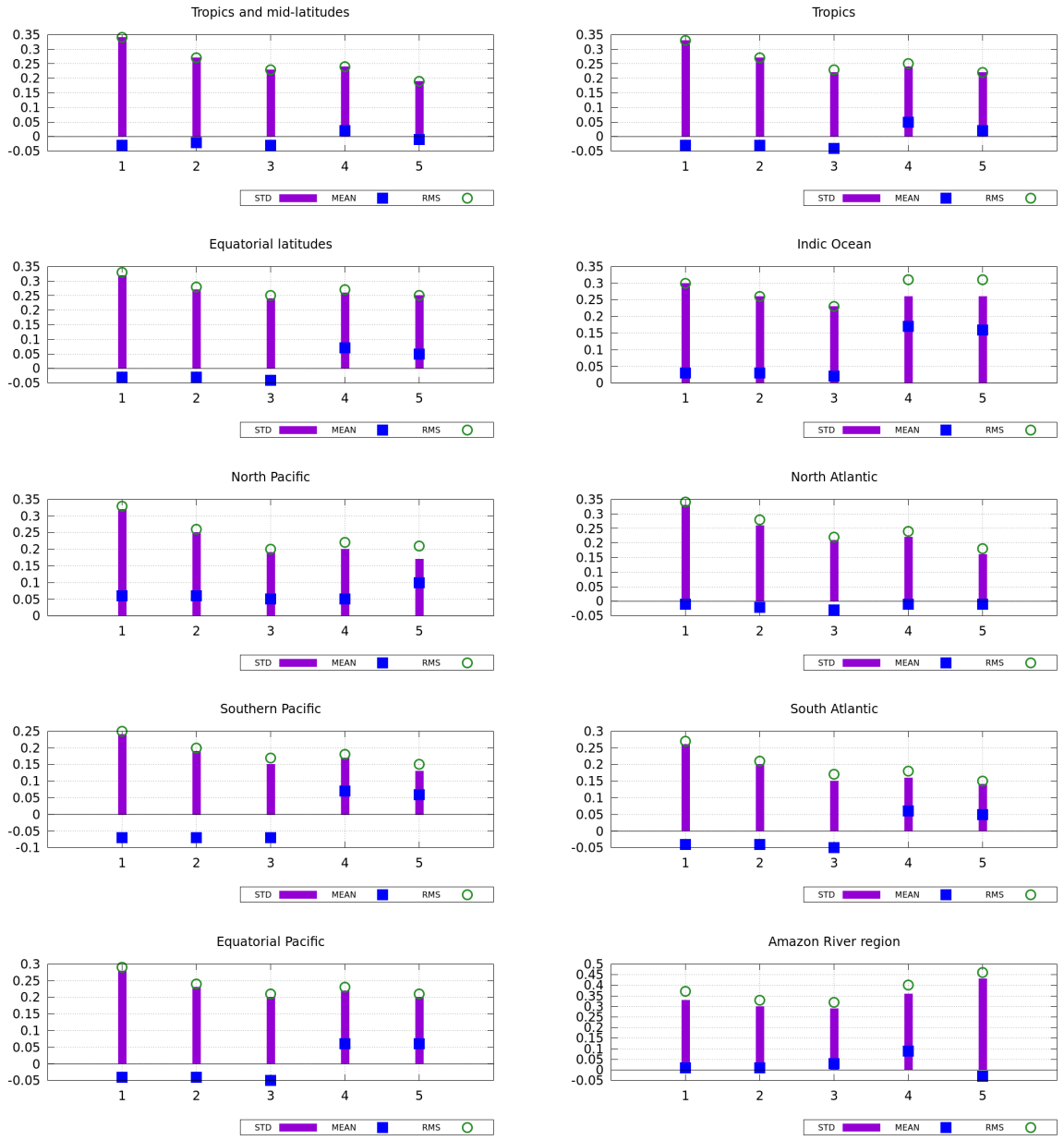

Figure 6: Regional statistics of differences of the different SMOS BEC SSS with respect to Argo salinity for the year 2013. Index 1 corresponds to the statistics of HR; 2 corresponds to LR; 3 to L4; 4 to L3V1; and 5 to L4V1.

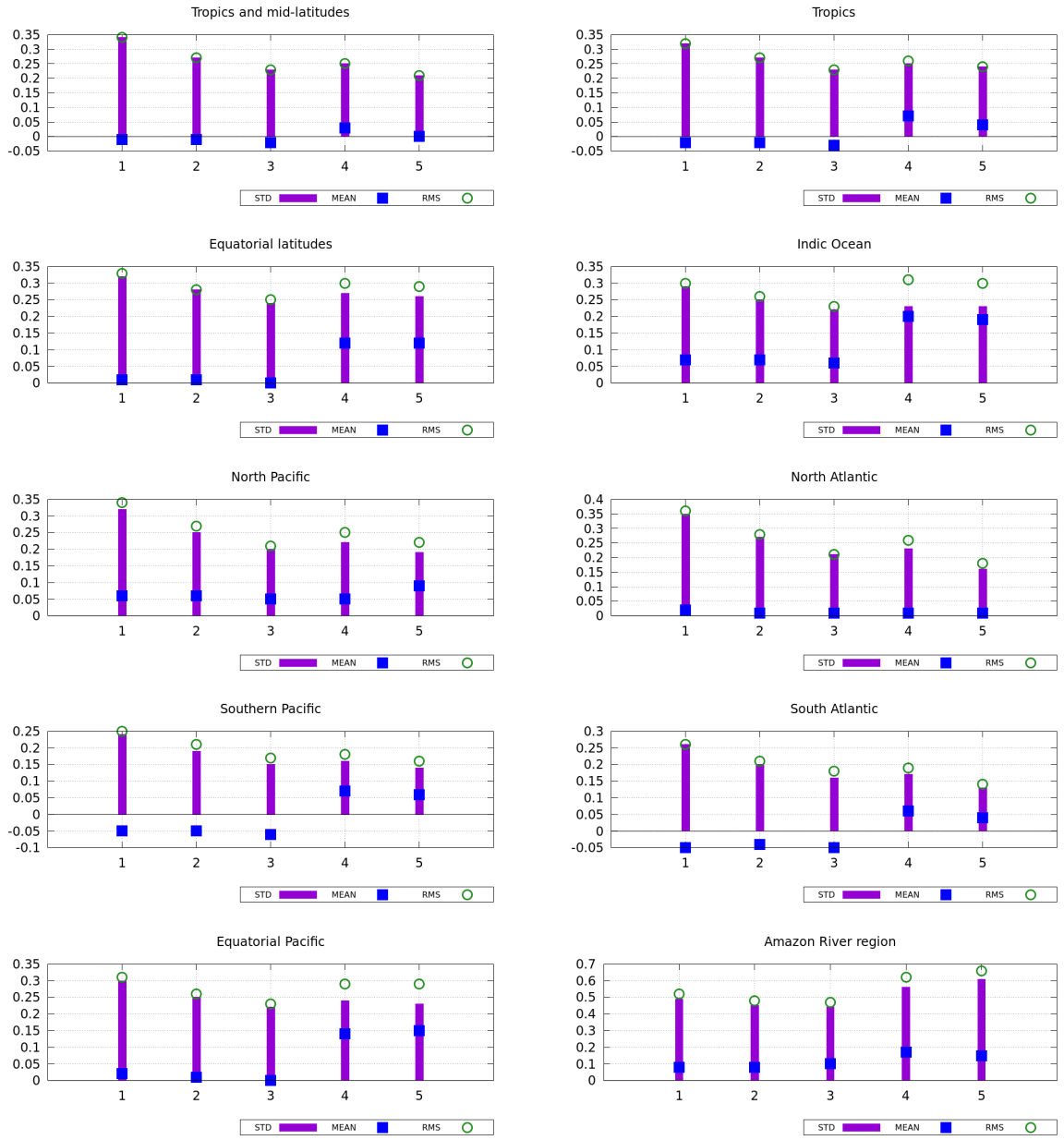

Figure 7: Regional statistics of differences of the different SMOS BEC SSS with respect to Argo salinity for the year 2014. Index 1 corresponds to the statistics of HR; 2 corresponds to LR; 3 to L4; 4 to L3V1; and 5 to L4V1.

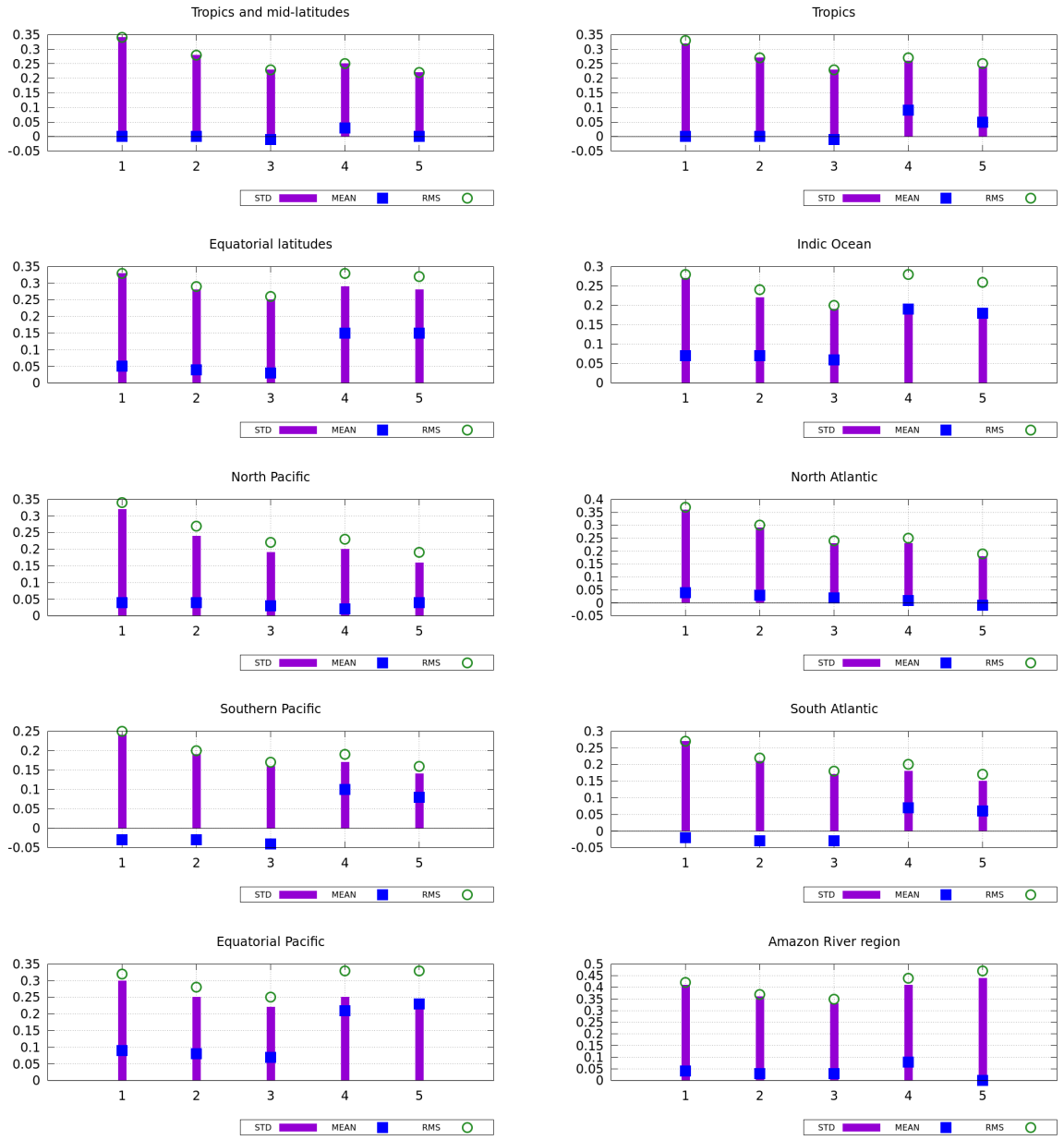

Figure 8: Regional statistics of differences of the different SMOS BEC SSS with respect to Argo salinity for the year 2015. Index 1 corresponds to the statistics of HR; 2 corresponds to LR; 3 to L4; 4 to L3V1; and 5 to L4V1.

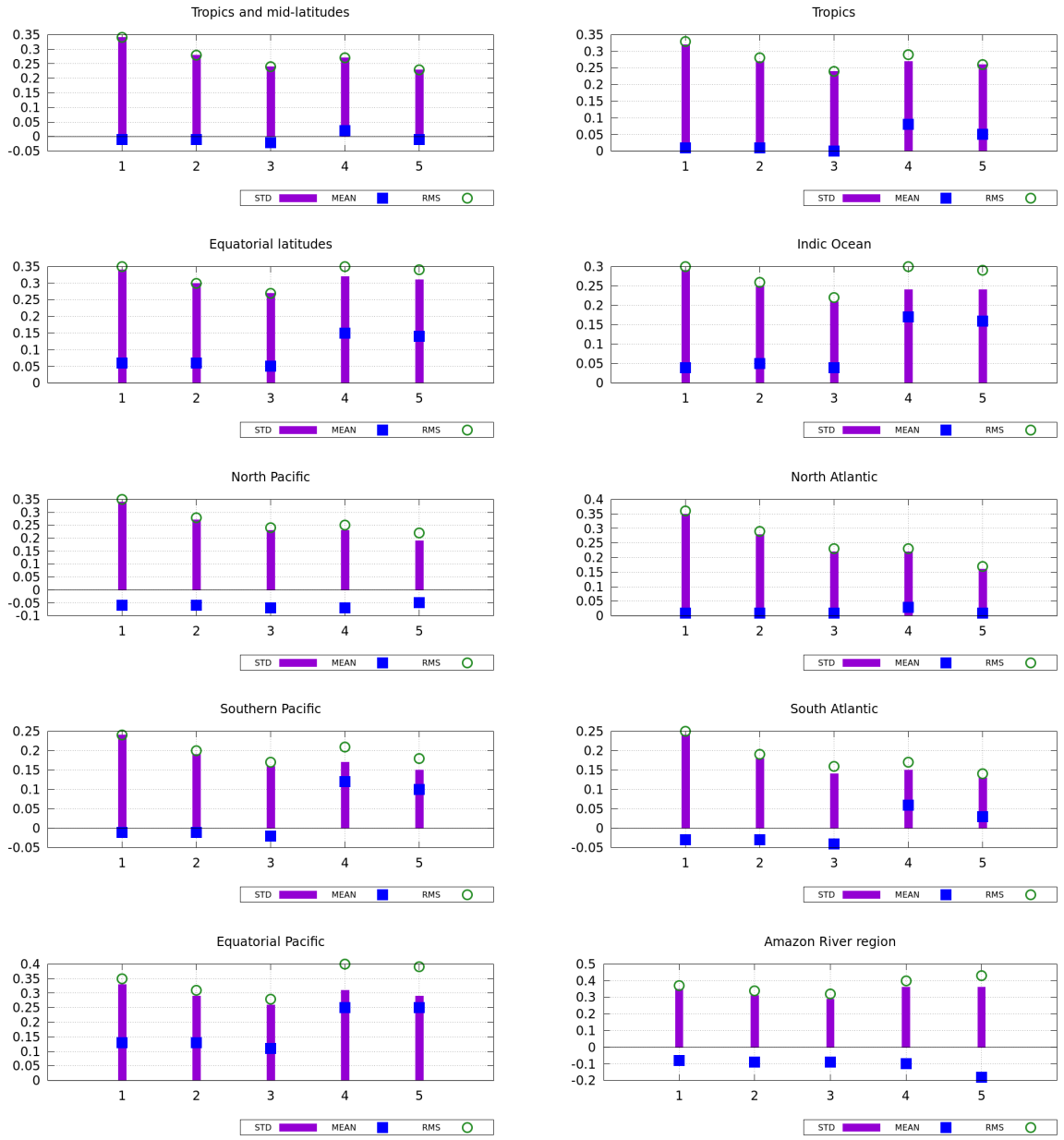

Figure 9: Regional statistics of differences of the different SMOS BEC SSS with respect to Argo salinity for the year 2016. Index 1 corresponds to the statistics of HR; 2 corresponds to LR; 3 to L4; 4 to L3V1; and 5 to L4V1.

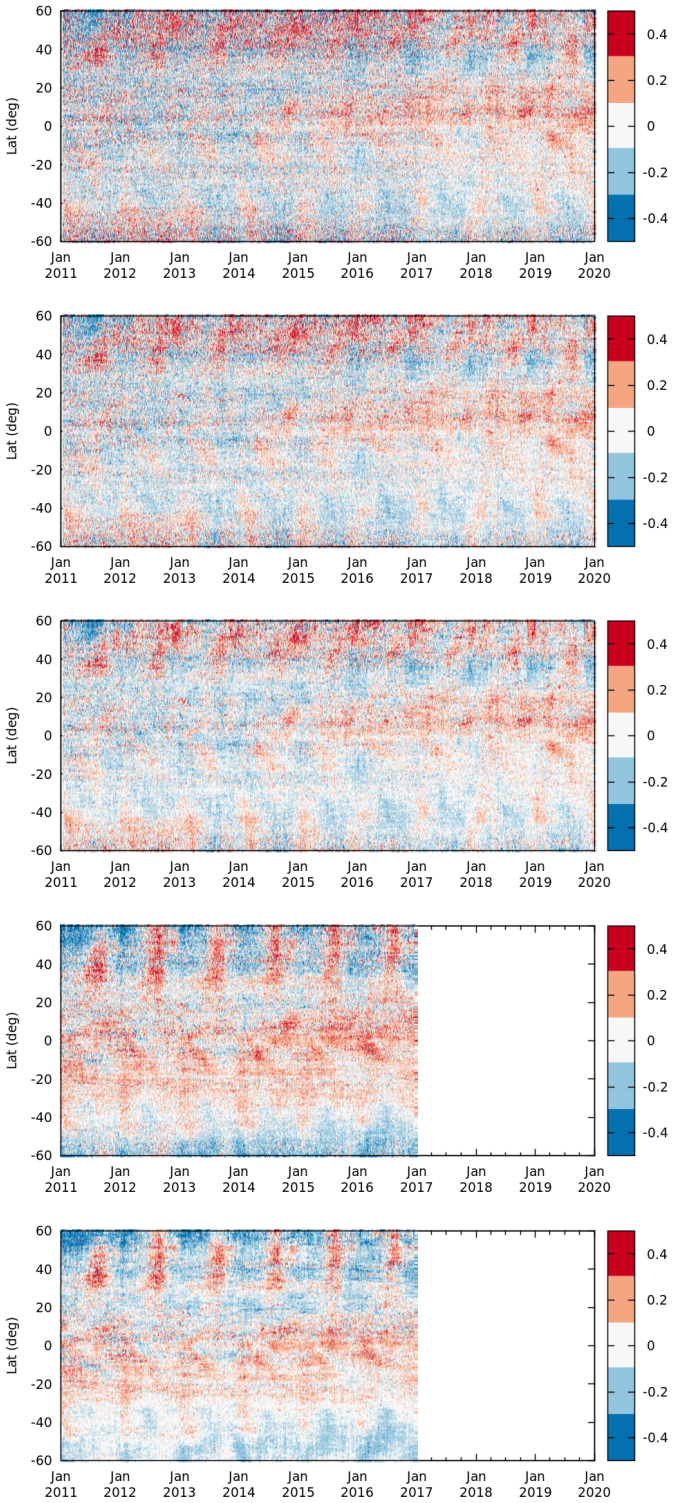

Figure 10: Hovmoller plots showing the temporal evolution of the mean differences between SMOS and Argo in latitudinal bands of 0.25^o. From top to bottom: first plot corresponds to the differences between HR and Argo; second to LR minus Argo; third L4 minus Argo; forth L3V1 minus Argo; and last plot corresponds to the differences between L4V1 and Argo.

Figure 11 shows the temporal evolution of the mean differences between SMOS and Argo for each region defined in Table 2 and Figure 12 the standard deviation of the differences between SMOS and Argo in the same regions. In 2017 there is a decrease of the standard deviation of the differences SMOS minus Argo that is specially relevant for the HR product in the GLO region. The rest of products (LR and L4) also present a decrease of the standard deviation from 2017 on, but it is not so large (probably because of the smoothing effects of the interpolation algorithms used in their generation). We have further investigated whether this decrease of standard deviation is associated to an improvement of the quality of the maps.

First, the spatial distribution of the standard deviations of the differences between HR and Argo (see Figure 13) shows the decrease of the standard deviation of 2017 with respect to 2015 in the entire ocean, but it is specially relevant in the Chinese Sea and Indian ocean.

In order to get a deeper insight in the origin of the observed reduction of the standard deviation of the differences with respect to in situ data from ARGO, we have computed the SMOS climatological histograms for two different 3 year period comprising: (i) 2011-2013 for a larger standard deviation period and (ii) 2017-2019 for a lower standard deviation. It allows us to check if the reduction of the standard deviation of the differences is already present in the SMOS measurements, or it is due to the methods used in the generation of the product. Figure 14 shows the standard deviation of these histograms for ascending orbits and acquisition conditions in the center of the swath and incidence angle of 42^o. We observe a significant decrease of the standard deviation in the entire Euro-Asian coast. These regions are specially affected by RFI. The decrease of the standard deviation in those regions suggests that the affectation of RFI have decreased during the last past years. The top plot in figure 15 shows the difference between the previous two maps. Although the largest differences are close to the Euro-Asian coast, the global ocean also presents a decrease in the standard deviation of the salinity the last years. The same occurs in the case of descending orbits (see bottom plot in figure 15).

To get a deeper insight whether the reduction of the standard deviation in the Euro-Asian coast is due to the decrease of RFI sources, we show the maps of probability of RFI affectation over land distributed by CESBIO for a 15-day period (see Figure 16). On the top row the two maps correspond to the year 2013, the 25th of February, on the left for ascending orbits and on the right for descending orbits. On the bottom plots, the two plots correspond to the same 15 days period but in 2019 (left ascending and right descending). The affectation by RFI located on the continent covers practically the entire coast. In 2019 a reduction of the RFI probability is observed, specially in China. We observe an increase in 2019 of the affectation of RFI. This increase is also reflected in the map of differences between the standard deviation of the two SMOS climatological historgams (see Figure 15, the blue regions in the African coast).

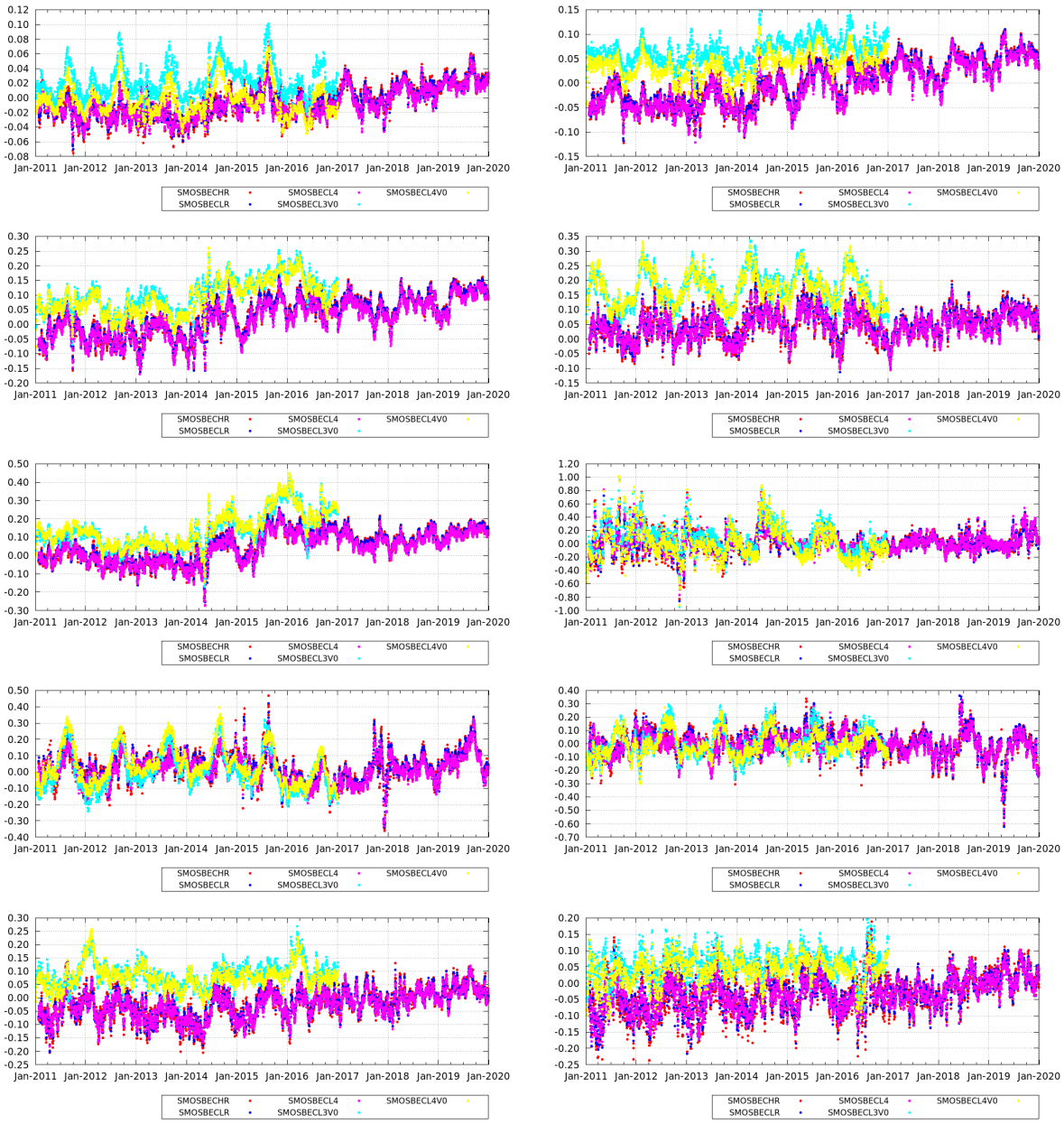

Figure 11: Time evolution of the mean differences between SMOS and Argo in different ocean regions from top to bottom and left to right: First row: GLO and TRO; second row EQU and IND; third row EPAC and EAT; forth row NPAC and NAT; fifth row SPAC and SAT.

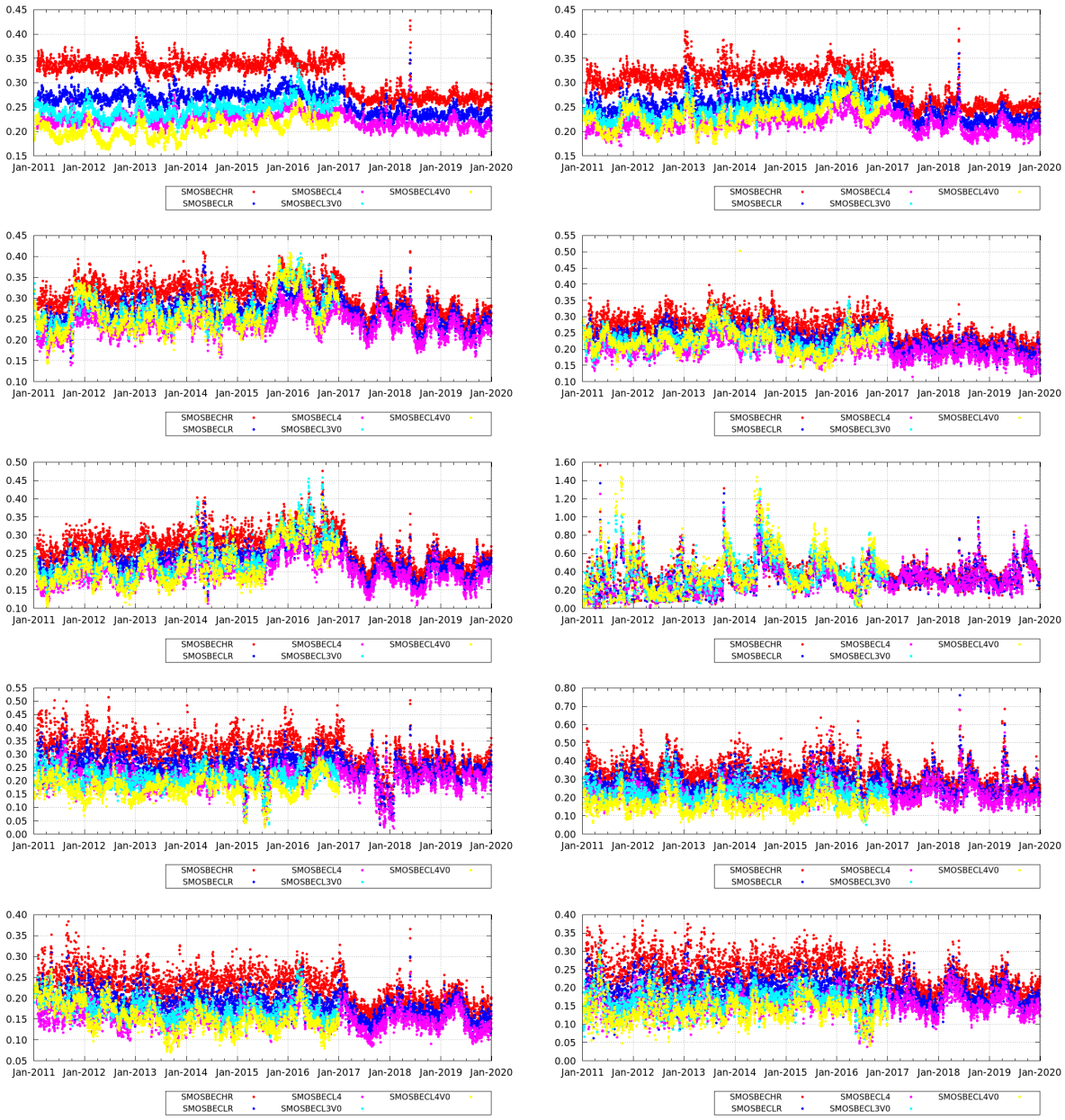

Figure 12: Time evolution of the standard deviation differences between SMOS and Argo in different ocean regions from top to bottom and left to right: First row: GLO and TRO; second row EQU and IND; third row EPAC and EAT; forth row NPAC and NAT; fifth row SPAC and SAT.

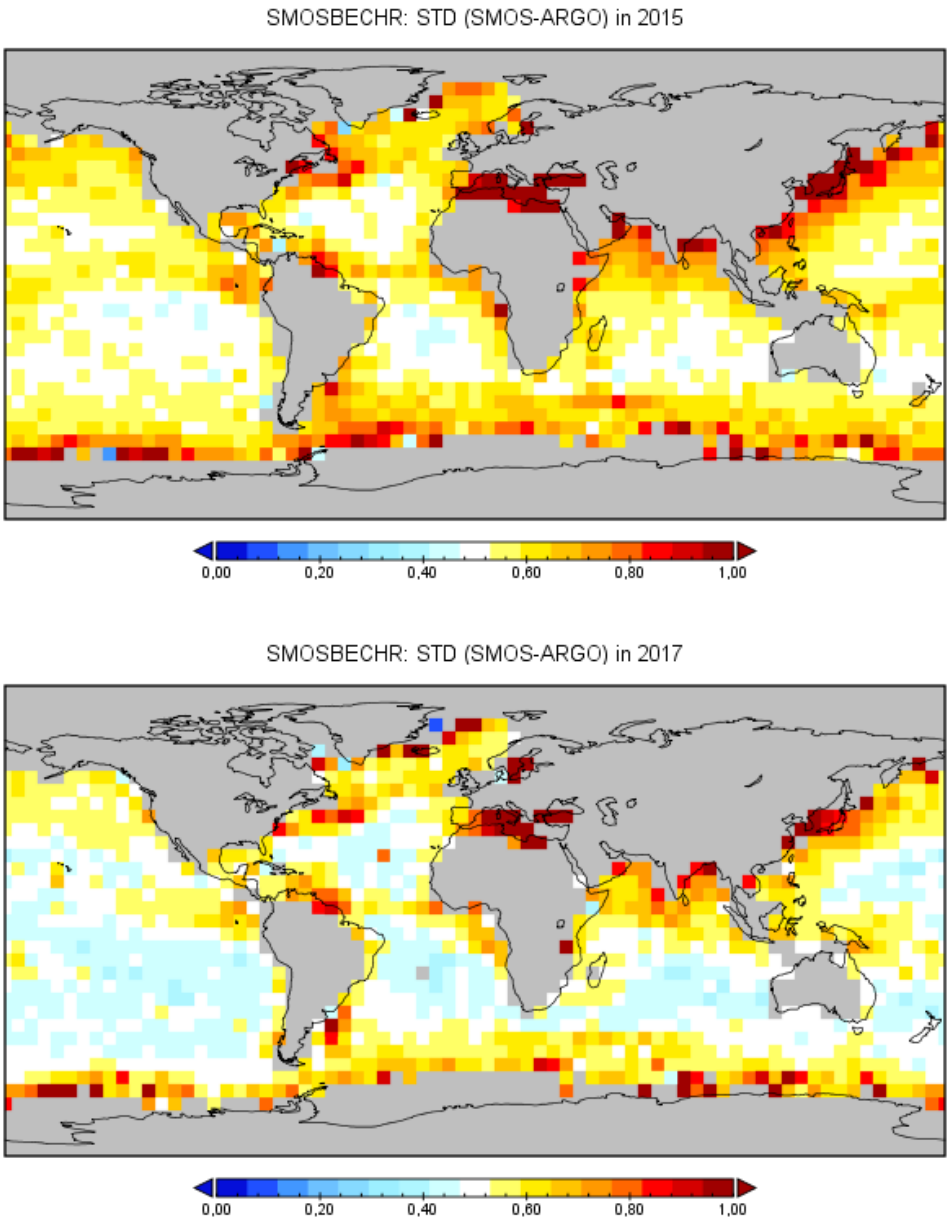

Figure 13: Spatial distribution of the standard deviation of the differences between SMOS HR and Argo salinity. Differences are accumulated in cells of $5^o \times 5^o$ along one year: Top plot corresponds to the year 2015; and bottom plot corresponds to the year 2017.

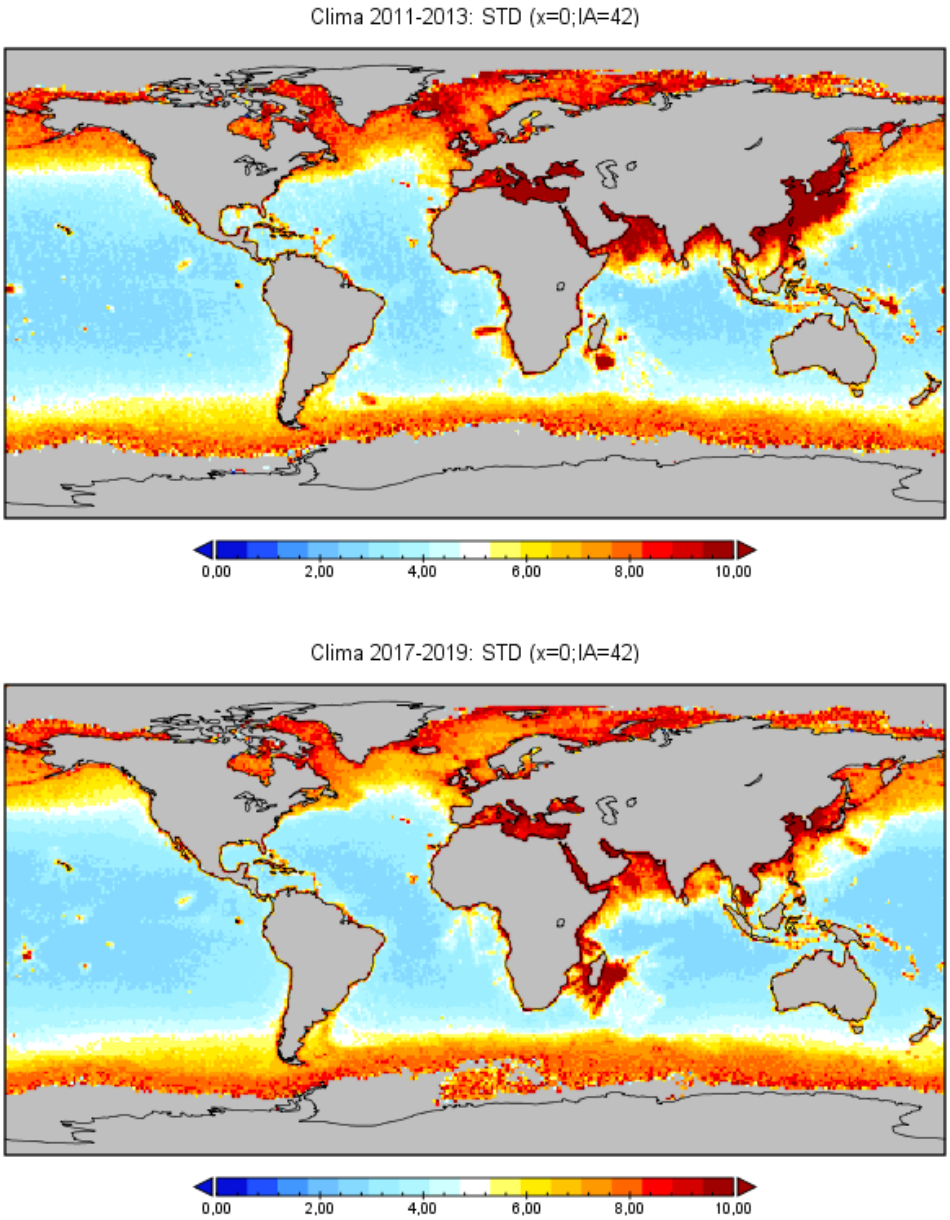

Figure 14: Standard deviation of the SMOS-based climatologies for ascending orbits, in the center of the swath and for incidences angles of 42^o in two cases: on the top the SMOS-based climatology is computed by using measurements in years 2011, 2012 and 2013; on the bottom the SMOS-based climatology is computed by using measurements in 2017, 2018 and 2019.

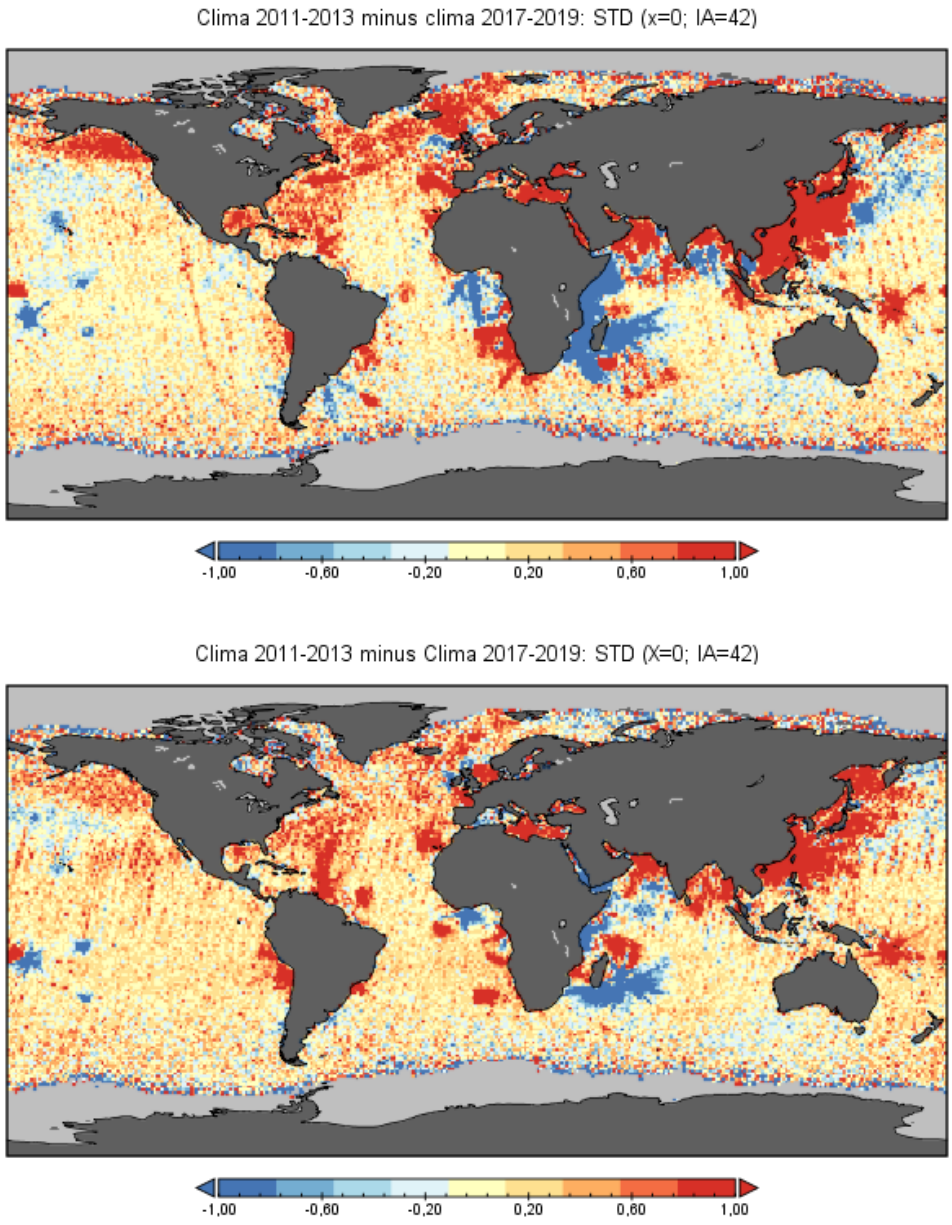

Figure 15: Differences in the standard deviation of the SMOS-based climatologies computed from 2011-2013 and from 2017-2018. The plots correspond to the center of the swath and for incidences angles of 42^o for ascending orbits (top) and descending orbits (bottom).

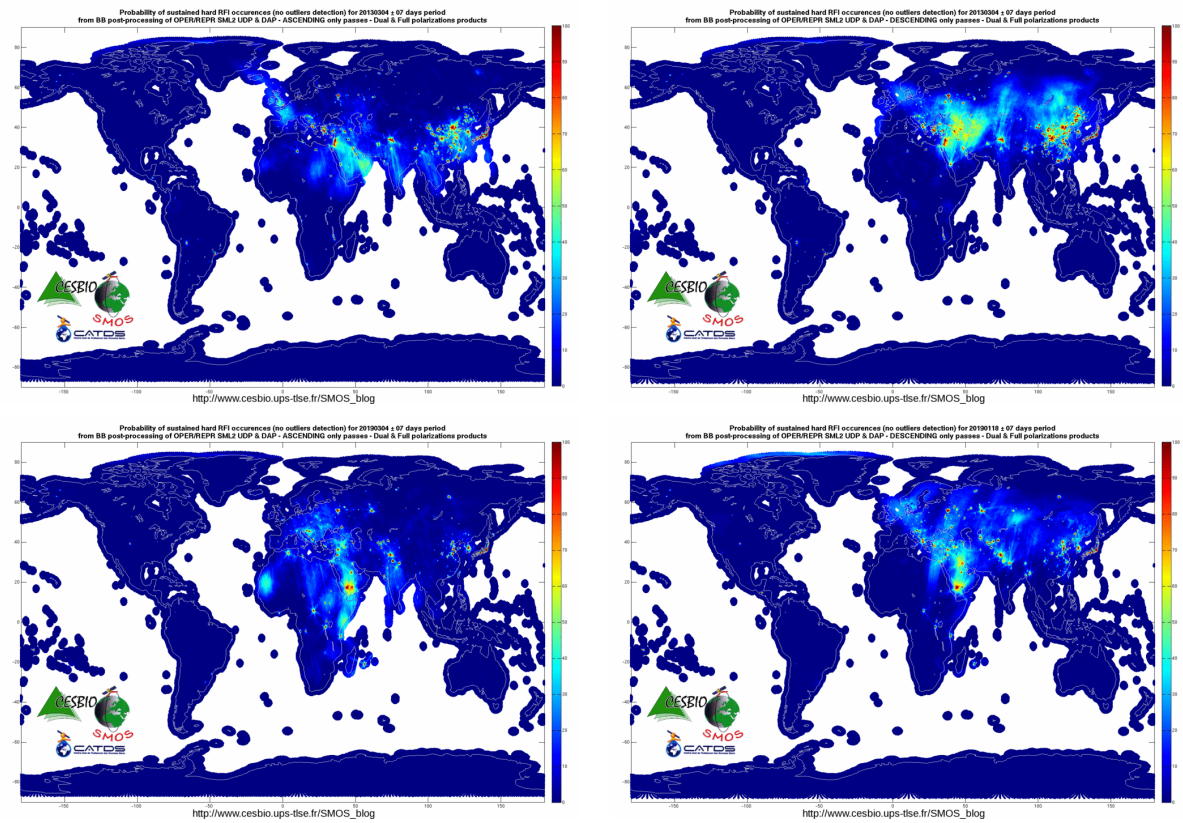

Figure 16: 15-day maps (centered in th 25th February) of probability of affectation of RFI over land distributed by CESBIO. Top left: ascending orbits in 2013; top right: descending orbits in 2013; bottom right: ascending orbits in 2019: bottom left: descending orbits in 2019. The most of RFI sources are located in the Euro-Asian continent and thus degrade the quality of the measurements in entire Euro-Asian coast. The year 2019 a reduction of RFI affectation is observed.

References

[Deimos, 2014] Deimos (2014). *SMOS L1 Processor L1C Data Prorocessing Model. SO-DS-DME-L1PP-0009*. Deimos. version 2.14.

[Donlon et al., 2012] Donlon, C. J., Martin, M., Stark, J., Roberts-Jones, J., Fiedler, E., and Wimmer, W. (2012). The operational sea surface temperature and sea ice analysis (ostia) system. *Remote Sensing and Enviroment*, 116(0):140 – 158.

[ESA, 2014] ESA (2014). Earth Observation CFI v3.x branch. http://eop-cfi.esa.int/index.php/mission-cfi-software/eocfi-software/branch-3-x. [Online; accessed 23-August-2016].

[Freitas, 2013] Freitas, S. (2013). *ECMWF v316 Update Analysis. SO-TN-DME-ECMWF-001*. DEIMOS Engengaria.

[Guimbard et al., 2012] Guimbard, S., Gourrion, J., Portabella, P., Turiel, A., Gabarró, C., and Font, J. (2012). SMOS Semi-Empirical Ocean Forward Model Adjustement. *IEEE Trans. Geosci. Remote Sens., vol. 50, no. 5. pp. 1676-1687.*

[Klein and Swift, 1977] Klein, L. A. and Swift, C. T. (1977). An improved model for the dialectric constant of sea water at microwave frequencies. *IEEE Trans. on Antennas and Propagation*, 25:104–111.

[Martín-Neira et al., 2016] Martín-Neira, M., Oliva, R., Corbella, I., Torres, F., Duffo, N., Durán, I., Kainulainen, J., Closa, A., Zurita, A., Cabot, F., Khazaal, A., Anterrieau, E., Barbosa, J., Lopes, G., Tenerelli, J., Díez-García, R., Fauste, J., Martín-Porqueras, F., González, V., Turiel, A., Delwart, S., Crapolicchio, R., and Suess, M. (2016). SMOS Instrument performance and calibration after 5 years in orbit. *Remote Sensing of Environment*, 180:19–39.

[McMullan et al., 2008] McMullan, K. D., Brown, M., Martin-Neira, M., Rits, W., Ekholm, S., Marti, J., and Lemanczyk, J. (2008). SMOS: The Payload. *Geoscience and Remote Sensing, IEEE Transactions on*, 46(3):594–605.

[National Oceanographic Data Center, 2013] National Oceanographic Data Center (2013). WOA 2013 V2 Data Access. https://www.nodc.noaa.gov/cgi-bin/OC5/woa13/woa13.pl. [Online; accessed 23-August-2016].

[Olmedo et al., 2019] Olmedo, E., GonzÃ¡lez-Gambau, V., MartÃnez, J., GonzÃ¡lez-Haro, C., Turiel, A., Portabella, M., Arias, M., Sabia, R., Oliva, R., and Corbella, I. (2019). Characterization and correction of the latitudinal and seasonal bias in bec smos sea surface salinity maps. In *IGARSS 2019 - 2019 IEEE International Geoscience and Remote Sensing Symposium*, pages 7932–7935.

[Olmedo et al., 2016] Olmedo, E., Martínez, J., Umbert, M., Hoareau, N., Portabella, M., Ballabrera-Poy, J., and Turiel, A. (2016). Improving time and space resolution of smos salinity maps using multifractal fusion. *Remote Sensing of Enviroment*.

[Olmedo et al., 2017] Olmedo, E., MartÃnez, J., Turiel, A., Ballabrera-Poy, J., and Portabella, M. (2017). Debiased non-bayesian retrieval: A novel approach to smos sea surface salinity. *Remote Sensing of Environment*, 193:103 – 126.

[Reul et al., 2007] Reul, N., Tenerelli, J., Chapron, B., and Waldteufel, P. (2007). Modeling Sun glitter at L-band for sea surface salinity remote sensing with SMOS. *IEEE Trans. Geosci. Remote Sens.*, 45:2073–2087.

[Sabater and De Rosnay, 2010] Sabater, J. and De Rosnay, P. (2010). Milestone 2 tech note - parts 1/2/3: Operational pre-processing chain, collocation software development and offline monitoring suite. Technical report, ECMWF.

[Tenerelli et al., 2008] Tenerelli, J. E., Reul, N., Mouche, A. A., and Chapron, B. (2008). Earth Viewing L Band Radiometer Sensing of Sea Surface Scattered Celestial Sky Radiation-Part I: General Characteristics. *Geoscience and Remote Sensing, IEEE Transactions on*, 46(3):659–674.

[Turiel et al., 2005] Turiel, A., Isern-Fontanet, J., Garcia-Ladona, E., and Font, J. (2005). Multifractal method for the instantaneous evaluation of the stream function in geophysical flows. *Phys. Rev. Lett.*, 95:104502.

[Turiel et al., 2008] Turiel, A., Yahia, H., and PÃ©rez-Vicente, C. J. (2008). Microcanonical multifractal formalism-a geometrical approach to multifractal systems: Part i. singularity analysis. *Journal of Physics A: Mathematical and Theoretical*, 41(1):015501.

[Umbert et al., 2014] Umbert, M., Hoareau, N. Turiel, A., and Ballabrera-Poy, J. (2014). New blending algorithm to synergize ocean variables: the case of SMOS sea surface salinity maps. *Remote Sensing of Environment 146, pp. 188-200.*

[Zweng et al., 2013] Zweng, M. M., Reagan, J. R., Antonov, J. I., Locarnini, R. A., Mishonov, A. V., Boyer, T. P., Garcia, H. E., Baranova, O. K., Johnson, D. R., Seidov, D., and Biddle, M. M. (2013). *World Ocean Atlas 2013, Volume 2: Salinity.* Levitus, Ed., A. Mishonov Technical Ed.; NOAA Atlas NESDIS 74, 39 pp.